This paper is a postprint of a paper submitted to and accepted for publication in IET Radar Sonar and Navigation and is subject to Institution of Engineering and Technology Copyright.
The copy of record is available at the IET Digital Library.

DVB-T based Passive Radar for simultaneous counter drone operations and civil air traffic surveillance

Tatiana Martelli [1*], Fabiola Colone [1], Roberta Cardinali [2]

[1] DIET Department, Sapienza University of Rome, Via Eudossiana 18, 00184 Rome, Italy
[2] Leonardo Company, Via Tiburtina Km 12.400, 00131 Rome, Italy
[*] tatiana.martelli@uniroma1.it

Abstract: The effectiveness of DVB-T based Passive Radar in counter drones operations is investigated in this paper aiming at monitoring airport terminal areas. In particular, we demonstrate that such sensors could be effectively employed to provide simultaneous short range surveillance against drones and long range monitoring of aircrafts from civil air traffic. To this purpose, several experimental tests have been performed with the DVB-T based AULOS® passive sensor developed by Leonardo S.p.A using very small RCS drones as cooperative targets along with conventional air traffic as targets of opportunity. An appropriate signal processing architecture is proposed for the two search tasks to be accomplished simultaneously. This is extensively applied against the collected datasets, based on the algorithmic solutions devised by the research group at Sapienza University. The reported results clearly prove the capability of a DVB-T based Passive Radar of simultaneously detecting and localizing drones flying around the airport area as well as the typical civil aircrafts at longer distances.

1. Introduction

Nowadays, the unmanned aerial vehicles (UAVs) and drones are being used for a wide variety of applications, including aerial photography and video, search and rescue operations and agriculture/environment monitoring. Nevertheless, beyond their harmless uses, civilian drones have been increasingly used in problematic ways creating personal privacy and public security issues [1]. In particular, these low flying objects are becoming a serious threat for the aviation safety and the airport security due to unauthorized drone activity. Recently, different collisions between aircrafts and drones have occurred and, more and more often, drones are sighted over the airport area causing the instant interruption of hundreds of scheduled flights and a huge inconvenience to the travellers [2]-[3].

Consequently, detection, tracking and classification of these particular objects have become key requirements for surveillance systems to protect airports as well as other critical infrastructure from hostile incursions. To this purpose, many anti-drone systems have been developed exploiting different sensing technologies, including audio, video, radio frequency (RF) and radar, [4]. Among them, indeed radar systems play an important role, thanks to their long-range, 24h all-weather monitoring capabilities. On the other hand, the unpredictable and complex motion of the targets of interest, along with the low Radar Cross Section (RCS), make the drone detection a challenging task for any radar system. Moreover, several restrictions exist for their installation in populated areas and/or any other site where electromagnetic emissions are limited by regulations in force.

In such scenarios, the Passive Radar (PR) technology represents a compelling alternative to the use of the conventional active radar systems. As a PR system does not have its own transmitter, this allows reduced costs, intrinsic covert operation capability and the lack of additional electromagnetic pollution [5].

With reference to the considered airport surveillance application, we focus on a specific advantage yielded by the PR operation that is the capability to provide simultaneous short and long range surveillance. Usually, such tasks are carried out by dedicated conventional radar systems, with the employed waveforms, the power budget, and the search strategies carefully tailored to the considered application.

Among the possible waveforms of opportunity, digital broadcast transmitters, such as the DVB-T emitters, are particularly attractive for applications requiring simultaneous short and long range surveillance. Thanks to the inherent bistatic configuration and the parasitic exploitation of continuous wave (CW) transmitters, DVB-T based PR sensors do not suffer from blind ranges effect typical of active monostatic pulse radar. By continuously emitting their signals, these transmitters provide a persistent illumination of the targets of interest. Moreover, the stationary nature and the isotropic characteristic of the employed illuminators of opportunity allow the PR receiver to exploit very long integration times to compensate for the limited power density generated by the emitter in order to widen the coverage area. Also, compared to other broadcast services, DVB-T transmitters provide a good range resolution to be effectively employed in short range applications.

The potential of a DVB-T based PR for Air Traffic Control (ATC) applications has been demonstrated in a number of studies [6]-[9]. Recently, the use of such sensor has been also investigated for the detection of small UAVs and drones [10]-[13].

In this paper we aim at demonstrating the effectiveness of DVB-T based PR in airport surveillance for the simultaneous detection of UAVs and drones at short ranges along with the conventional civil air traffic at farther distances. Following the preliminary promising results reported in [13], an extensive study is presented that includes more complex and realistic scenarios as well as advanced signal processing strategies.

This study is the result of an experimental activity carried out in cooperation with the colleagues of Leonardo S.p.A.. Specifically several experimental tests have been performed in a military airport using the DVB-T based

This paper is a postprint of a paper submitted to and accepted for publication in IET Radar Sonar and Navigation and is subject to Institution of Engineering and Technology Copyright.
The copy of record is available at the IET Digital Library.

AULOS® PR. One or two extremely small cooperative drones were employed, flying in the surrounding area of the airport at different distances from the passive sensor. Simultaneously, aircraft of civil air traffic have been considered as targets of opportunity at distances up to few hundreds of kilometres.

The processing scheme developed by the research group of Sapienza University of Rome and tailored for the twofold search task [13] has been extensively tested against the collected data sets. Moreover, it has been extended to take advantage of the frequency and spatial diversity allowed by the multi-frequency operation and a non-uniform linear array layout, [8], [14]. The results are reported both in terms of detection performance and localization capability for both the short and long surveillance tasks in order to demonstrate the effectiveness of the DVB-T based PR in the considered scenario.

The paper is organized as follows. Section 2 illustrates the scenario of interest. Section 3 describes the experimental test campaigns and the adopted processing scheme tailored for the twofold search task. The results obtained using the presented approach are reported in Section 4 for both short and long range targets. In Section 5 the processing scheme is extended to include the joint exploitation of frequency and spatial diversity and the resulting benefits on the achievable performance are illustrated in Section 6 by means of application to the available experimental datasets. Finally, our conclusions are drawn in Section 7.

2. Airport terminal area scenario and the role of passive radar

Due to the high-density traffic around the airport area, modern ATC and ground control systems are required to strengthen the airspace safety level and to enhance the security level in the proximity of an airport. To be effective, the technologies to be deployed in the airport terminal area should allow accurate detection and tracking of conventional air traffic also during the landing and take-off phases. In addition, a careful surveillance of the terminal area is required to prevent collisions and to avoid runway incursions from other aircraft, vehicles or people. In particular, the growing proliferation of UAVs and drones represents an emerging threat for airport security that cannot be ignored anymore.

In the context outlined above, the security level enabled by conventional active radar systems could be augmented by the cost-effective, nonintrusive, and eco-friendly PR technology. In fact, in order to guarantee a complete and continuous coverage, PR can be effectively integrated within conventional active radars to extend the surveillance coverage, acting as "gap-filler", but also to reduce the probability of out of service of the surveillance system. It is worth noticing that, aiming at the monitoring of airport terminal areas, where electromagnetic emissions are limited by regulations related to public safety and risk of interference with pre-existing systems, a network of passive sensors could be easily deployed to provide continuous and complete coverage.

As previously mentioned, the exploitation of the broadcast DVB-T transmitters represents one of the best choice for the considered application. Specifically, the high radiated power of these transmitters and the excellent coverage make them suitable for the detection of small RCS and low-altitude targets as well as for medium/long range air traffic surveillance applications. In addition, the continuous emissions and the fine range resolution of about 20 m (equivalent monostatic range resolution yield by a signal bandwidth of approximately 8 MHz) make them potentially able to continuously detect and discriminate closely spaced targets. In fact, aiming at the detection of the low signal to noise ratio (SNR) targets and at widening the DVB-T based PR coverage area, very long integration times (up to few seconds) can be exploited if the migration effects are properly compensated [9], [15]. It is worth noticing that the use of long integration time allows also to improve the Doppler resolution as well as the capability to discriminate between slowly moving targets and clutter contributions, which is of particular interest for the application under consideration, especially in the short range case due to the high-density traffic around the airport area. Eventually, by employing an OFDM modulation, the DVB-T signals are noise-like waveforms; thus, they provide ambiguity function with attractive properties that are nearly independent of the signal content and almost time-invariant [8].

Table 1. Values used in the SNR evaluation.

Parameters	Values
Equivalent Isotropic Radiated Power (EIRP)	50 kW
Receiver antenna gain (G_{RX})	15 dB
Wavelength (λ)	0.525 m
Aircraft target RCS (σ)	100 m^2
Drone target RCS (σ)	0.01 m^2
Coherent processing gain ($G_{int}@T_{int} = 0.5s$)	66.6 dB
Boltzmann constant (K)	$1.38 \cdot 10^{-23}$ J/K
Noise figure, including system loss (F)	25 dB
Receiver bandwidth (B)	7.61 MHz
System temperature (T_0)	290 K

In order to provide a preliminary evaluation of the expected coverage of such sensors against drones and aircraft, a power budget analysis is reported below. By resorting to the well-known bistatic radar equation [16], the signal-to-noise ratio (SNR) for a given target can be expressed as:

$$SNR = \frac{EIRP \cdot G_{RX} \cdot \lambda^2 \cdot \sigma}{(4\pi)^3 \cdot R_{TX}^2 \cdot R_{RX}^2 \cdot KT_0FB} G_{int} \qquad (1)$$

where R_{TX} is the transmitter-target distance, R_{RX} is receiver-target distance while Table 1 provides all the other definitions and values adopted for the parameters appearing in eq. (1). Notice that the numerical values as well as the bistatic radar geometry have been selected to be identical or close enough to those characterizing the experimental tests reported in the subsequent Sections.

Fig. 1(a-b) show the expected SNR map across the surveyed area when a big sized target (RCS=100 m^2) and a small RCS target (RCS=0.01 m^2) are considered, respectively. In both case studies, we report the results over a square region whose dimensions are selected according to the considered

This paper is a postprint of a paper submitted to and accepted for publication in IET Radar Sonar and Navigation and is subject to Institution of Engineering and Technology Copyright.
The copy of record is available at the IET Digital Library.

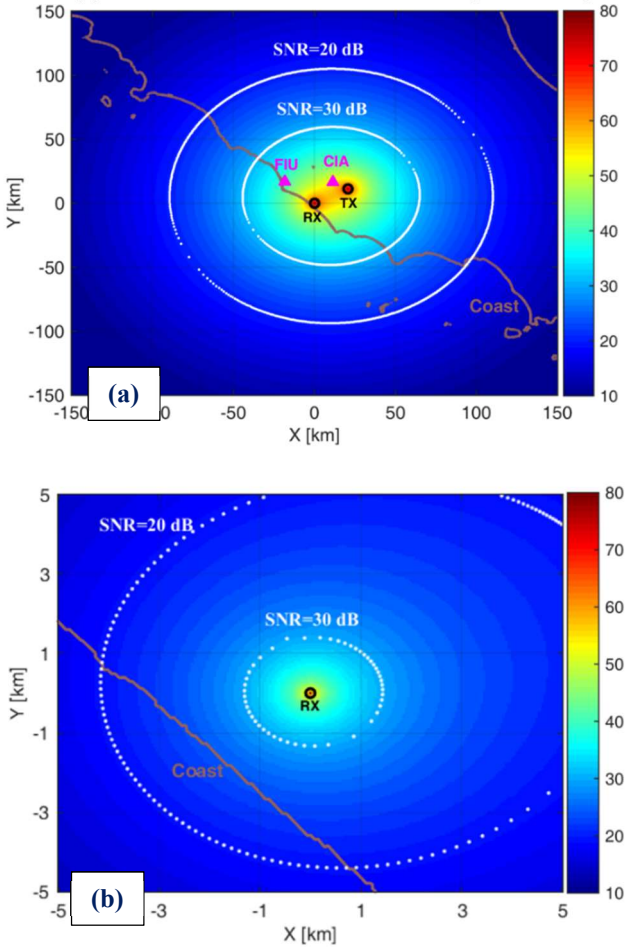

Fig. 1. *Theoretical SNR at different distances from the DVB-T based PR against: (a) big sized aircraft; (b) small drones.*

surveillance task. The position of the RX sets the axes origin which is assumed to be sited within the airport and the TX lies at $(X, Y) = (20.8, 11.3) km$.

By observing Fig. 1(a) we notice that, in principle, aircraft could be detected up to several tens of kilometres from the receiver with a high probability of detection for typical values of probability of false alarm (P_{fa}). Simultaneously, based on the SNR values in Fig. 1(b), small drones flying around the airport area could be detected with good probability at distances up to 4-5 kilometers from the PR sensor.

Notice that, the reported theoretical coverages have been obtained using a reference integration time of 0.5 s (see Table 1). Based on the coverage extent required in civil air traffic surveillance applications, we observe that such integration time value is strictly necessary and should be potentially extended in the case of wide area aerial surveillance. In contrast, aiming at the detection of drones, the considered integration time is suitable for distances up a few kilometers from the PR sensor. Obviously, also against the drones, a longer integration time could be exploited to further widen the coverage or to improve the detection of lower RCS targets. However, notice that the resulting integration gain could be upper limited by the coherency of the target echoes. Moreover the increase of the integration time should be traded for a reduced update rate of the system, which is a strategic aspect when dealing with rapidly maneuvering UAVs.

It is worth mentioning that this theoretical analysis does not take into account the direct signal from the TX and the returns from the stationary scene, assuming ideally that these contributions have been perfectly removed by dedicated signal processing stages that is able to restore a noise-limited condition. Similarly, the coherent integration gain has been set independently of the effectiveness of the techniques implemented to enable the exploited integration times, against typical migration effects of the targets of interest.

In practice, several factors could limit the performance of the conceived sensor with respect to the above expectations. Therefore, an experimental validation is essential to demonstrate the suitability of a DVB-T based PR in the airport terminal area scenario.

3. Experimental campaign and signal processing scheme

In this section, we describe the experimental tests performed in February and March 2019 in cooperation with the colleagues of Leonardo S.p.A. and we illustrate the signal processing scheme that has been extensively used for a preliminary analysis of the achievable performance.

A. Experimental tests description

Dedicated test campaigns were carried out at the military airport of Pratica di Mare Airport (Rome, Italy), using the DVB-T based AULOS® passive sensor. The acquisition geometry is sketched in Fig. 2. The DVB-T transmitter of Monte Cavo (22.5 km away) was exploited as illuminator of opportunity while the DVB-T based PR receiver was installed close to the runway of the airport (see the enlarged view of the local geometry on the bottom left corner of Fig. 2). Two or three Yagi-Uda surveillance antennas were employed during the performed tests, each one with a main beam width of 36^0. They were displaced in the horizontal plane according to different layouts. In this paper, wee report the results obtained with two surveillance antennas configurations exploiting either (i) two receiving antennas mounted at distance $d = 0.63\, m$ or (ii) a non-uniform linear array composed by three antennas with inter-element distances equal to $0.63\, m$ and $0.95\, m$, respectively.

Several datasets have been collected, each composed by sequential data files (namely scans). In this paper, we focus on three datasets. The number of scans, the temporal duration of each scan and the total acquisition time of each dataset are synthesized in Table 2. One or two DVB-T frequency channels have been simultaneously collected at carrier frequency F0=570 MHz and F1=754 MHz, both emitted by the same transmitter. Table 2 reports the exploited DVB-T channels for each dataset.

During the test campaigns, one or two very small drones were employed as cooperative targets (see Fig. 3) flying in the surrounding area of the airport. They were a DJI Phantom 4 Pro of size approx. 25 cm x 25 cm (propellers excluded) and a DJI Mavic Pro of size approx. 20 cm long and 8.3 cm wide (propellers excluded). In the test campaigns, both drones were equipped with a GPS receiver in order to record their position. In Fig. 2, the green and red plots represent the GPS trajectories of the Phantom and the Mavic

This paper is a postprint of a paper submitted to and accepted for publication in IET Radar Sonar and Navigation and is subject to Institution of Engineering and Technology Copyright.
The copy of record is available at the IET Digital Library.

Fig. 2. *Sketch of the acquisition geometry.*

during the collected datasets, respectively. Moreover live ATC registrations of the aircraft present in the same area have been also collected.

Two different test area have been considered for the counter drone application. The centre of the first area is ideally located at a distance of about 1.7 km away from the RX (Test area 1 in Fig. 2), and the two drones flew along various paths reaching a minimum distance of 0.85 km up to a maximum distance of 1.93 km from the RX site. In the second case, the small flying objects flew up to the allowed boundaries of the airport area, yielding a maximum distance from the RX of approximately 3 km (Test area 2 in Fig. 2). In all cases, the surveillance antennas were appropriately pointed in order to include in the main beam the small flying objects as well as the many civilian air traffic departing or arriving to the Fiumicino airport. In Table 2, for each dataset reported in this paper, we detail the considered test area, the employed drones and the number of surveillance antennas exploited.

B. DVB-T based PR signal processing architecture for simultaneous surveillance of drones and aircraft

All the available data files underwent the DVB-T based PR processing scheme for target detection and localization developed by the authors and presented in [8]-[9]. Specifically, as illustrated in Fig. 4, in order to develop the joint short and long surveillance capability, the collected data are simultaneously forwarded to two parallel processing chains that are tailored to maximize the performance against the cooperative drones (at short range) and the civil air traffic at farther ranges, respectively. This approach is basically enabled by the characteristics of the DVB-T signals previously discussed and by the exploitation of software-defined radio (SDR) receiver architectures. In fact this implies the signal processing to be entirely digital so that it can be flexibly adapted to meet the requirements of different search tasks.

As it is apparent from Fig. 4, the two processing chains

(a)

(b)

Fig. 3. *Picture of the drone used as cooperative target: (a) DJI Phantom 4 Pro; (b) DJI Mavic Pro.*

are made up of the same blocks. Nevertheless, the algorithms implemented in each block together with the relevant parameters are properly adapted to the considered application. This might also include the timings to be employed (i.e. coherent integration intervals, update rates, time windows used for cancellation, etc.), which can be asynchronously set at the two processing chains to suit the needs of different tasks.

This paper is a postprint of a paper submitted to and accepted for publication in IET Radar Sonar and Navigation and is subject to Institution of Engineering and Technology Copyright.
The copy of record is available at the IET Digital Library.

The main required processing stages are briefly illustrated in the following together with the choice made for the parameters settings.

Table 2. Details of the data sets collected during the performed tests campaigns.

Dataset #	N° of drones	N° of scan	Scan duration	Scan distance	Total time duration	Frequencies	N° of surv	Test area [min max] distance
1	2	107	0.6 s	4.25 s	≈ 8 min	F0=570 MHz F1=754 MHz	3	1 [0.85 1.79] km
2	2	195	1.4 s	5.3 s	≈ 17 min	F0=570 MHz F1=754 MHz	3	2 [2.15 3.18] km
3	1 (Phantom)	147	1.4 s	2.75 s	≈ 7 min	F0=570 MHz	2	1 [1.45 1.93] km

Disturbance cancellation. First of all, we perform the removal of the undesired contributions in the surveillance channels, i.e. direct signal, clutter and multipath echoes. In both cases, we resort to the sliding version of the extensive cancellation algorithm (ECA-S) [17]. In fact, as widely demonstrated in [17], the ECA-S approach allows a good trade-off between disturbance cancellation and the capability to preserve low-velocity target echoes. To this aim, we recall that the batch duration T_B is selected to obtain remarkable cancellation performance while preserving targets moving at the minimum Doppler of interest (notch Doppler extension $\Delta f_n = 1/T_B$). In contrast, T_S is selected in order to move out of the velocity range of interest the undesired structures that arise from the batch processing of the received signals. By setting the maximum velocity, the filter update rate T_S depend on the exploited DVB-T channel, [17].

Based on the above considerations, we adopt batches of small dimensions against aerial targets to synthesize a wide Doppler cancellation notch to effectively remove the non-stationary disturbance. Differently, aiming at the detection of slowly moving objects with low RCS, longer batches are to be preferred to yield a narrower cancellation notch thus preserving the target echo. Therefore, aiming at long range aerial surveillance, the ECA-S operates over a range of 33 km with a batch duration T_B=0.1 s (i.e. Δf_n=10 Hz). Then, assuming a maximum velocity of 420 m/s, we might set T_S=0.6 ms and T_S=0.47 ms for the DVB-T channels at 570 MHz and 754 MHz, respectively. Instead, within the processing chain devoted to the detection of drones, the ECA-S operates over a range of 6 km with T_B=0.2 s (i.e. Δf_n=5 Hz). Finally, the maximum observed velocity can be limited at 50 m/s, so that T_S=5.2 ms and T_S=3.9 ms for F0=570 MHz and F1=754 MHz, respectively.

Range/Velocity map evaluation. After the cancellation stage, the output signals from ECA-S filter and the corresponding reference signals are used in order to evaluate the bistatic range-velocity maps. Notice that the reference signal is properly filtered before it is employed in such stage in order to remove the high side-lobes and spurious peaks appearing in the DVB-T signal ambiguity function. To this purpose, we resort to the approach presented in [18] which is based on the cascade of two filters, namely the pilot signals equalization and the Residual Peaks Removal (RPR) to remove the zero-Doppler peaks. It is worth noticing that both filters are not strictly necessary in the short range case since the spurious peaks appears outside the observed range/velocity region. Alternatively, the mismatching described in [18] can be applied once against the reference signal that is then exploited in both the processing chains. This also guarantees that the surveillance range/velocity area observed in short range applications is not affect by undesired structures arising from the presence of strong targets outside that area.

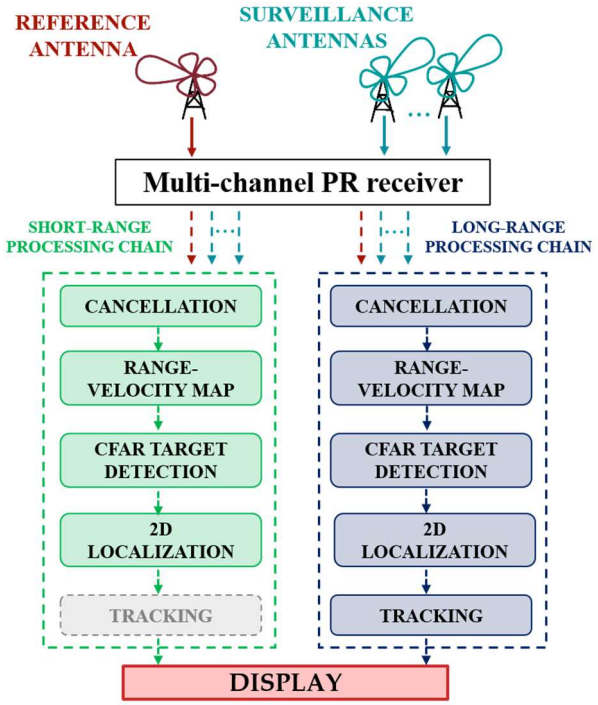

Fig. 4. *DVB-T based processing scheme for simultaneous detection and localization of drones and aircraft.*

The two different surveillance applications require different range-velocity map algorithms as well as different coherent integration times T_{int} values. In fact, in the aerial surveillance application case, aiming at increasing the detection capability of low RCS aircraft as well as at widening the coverage area, long T_{int} should be considered. In principle, extended T_{int} up to a few seconds could be exploited if the target range and Doppler migration effects are effectively compensated, [9],[15]. In this work, we use T_{int} values up to 1.2 s since the maximum data file temporal duration is 1.4 s (see Table 2, Datasets 2 and 3). In the reported experimental tests, since the aerial targets move with a dominant radial velocity component, only the range walk

This paper is a postprint of a paper submitted to and accepted for publication in IET Radar Sonar and Navigation and is subject to Institution of Engineering and Technology Copyright.
The copy of record is available at the IET Digital Library.

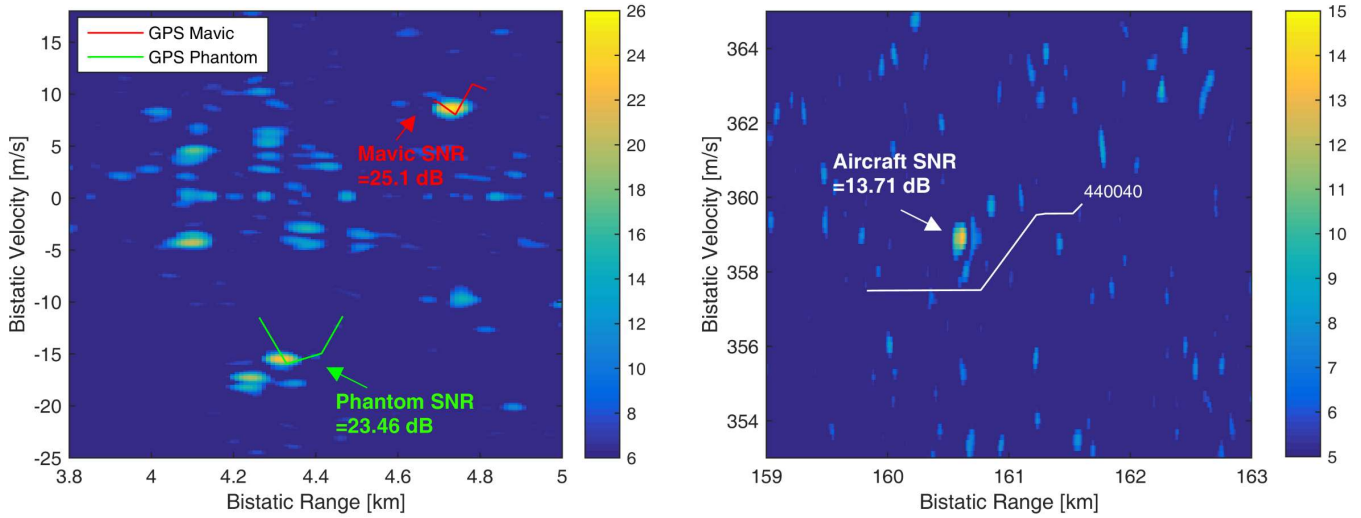

Fig. 5. *Dataset2: Enlarged view of the bistatic range-velocity maps obtained at the same scan against the: (a) drones; (b) aircraft.*

effects has to be compensated using the 1-LPI based KT approach proposed in [9]. When longer integration times are used or the target motion mostly includes cross-range trajectories, the approach proposed in [15] could be exploited to jointly compensate for range and Doppler walk effects.

In contrast, when short range surveillance is sought, due to the limited distances and low velocity of the targets of interest, slightly shorter integration times can be employed together with a conventional Correlation FFT algorithm (namely, without any compensation of the migration effects), [19]. Obviously, the T_{int} value strongly depends on the area to be monitored. Therefore, we set T_{int} =0.5 s and T_{int} =1 for datasets where the drones flew in Test area 1 and 2, respectively. In this case, a key requirement would be a high update rate which largely simplifies the tracking stage. To this purpose, efficient sub-optimal algorithms might be exploited for the evaluation of the range-Doppler map in real-time applications [19].

(a)

CFAR target detection. Once the range-velocity maps have been evaluated at all the available surveillance channels, a conventional Cell Average Constant False Alarm Rate (CA-CFAR) threshold is separately applied to each map to detect targets with a given probability of false alarm P_{fa}. Moreover, a M-out-of-K criterion can be applied to integrate the detection results obtained at the K surveillance channels. In the aerial surveillance application case, in order to extend the coverage, we operate with a final $P_{fa} = 10^{-6}$ on the Range-velocity plane and the CFAR threshold on each receiving channel is set accordingly. In contrast, in the short range case, due to the high density scenario and aiming at reducing the number of false alarms, we decide to operate with a final $P_{fa} = 10^{-7}$.

2D localization. Since multiple receiving antennas are available, once the target has been detected on the range-velocity plane, the Direction of Arrival (DoA) of the corresponding echo can be estimated. To this end, we adopt a conventional maximum likelihood (ML) approach. Obviously, for the case of two receiving antennas, the ML estimator corresponds to a simple interferometric approach. Eventually, the bistatic range and the DoA values are used to localize that targets in the Cartesian x-y plane.

Tracking. At the end, a tracking stage can be applied to reduce the false tracks while yielding more accurate measurements. Notice that, we adopt a conventional Kalman filter only in the aerial scenario case. This stage has not been applied against drones as they are characterized by a more complex and unpredictable motion, so that advanced tracking algorithms must be considered.

4. Experimental results

The signal processing architecture described in sub-section 3.B is now extensively applied to the available data sets. Before proceeding further, it is worth mentioning that the architecture in Fig. 4 provides the highest flexibility when fed with continuous time acquisitions because this would allow the timings (i.e. coherent integration intervals, update rates, time windows used for cancellation, etc.) to be asynchronously set at the two processing chains in order to suit the needs of different tasks. In contrast, in the following, it will be used against successive (temporally separated) data files as available from the performed tests (see sub-section 3.A). This does not allow to flexibly set the update rate for any of the two applications as this parameter is constrained by the data file separation especially when short acquisitions are collected in each file. Nevertheless, when longer data files are available, we emulate the continuous time acquisition by properly fragmenting the available registrations.

(b)

As a first example of the results obtained with the signal processing stages illustrated previously, Fig. 5(a)-(b) show the range-velocity maps obtained for a single data file (scan) from Dataset2 for the short and long range cases, respectively. Specifically, based on the availability of air truth information (namely, GPS or ADSB registrations), we report an enlarged view of the maps around the targets of interest. All the reported maps have been normalized to the thermal noise power level so that each value represents the estimated SNR.

This paper is a postprint of a paper submitted to and accepted for publication in IET Radar Sonar and Navigation and is subject to Institution of Engineering and Technology Copyright.
The copy of record is available at the IET Digital Library.

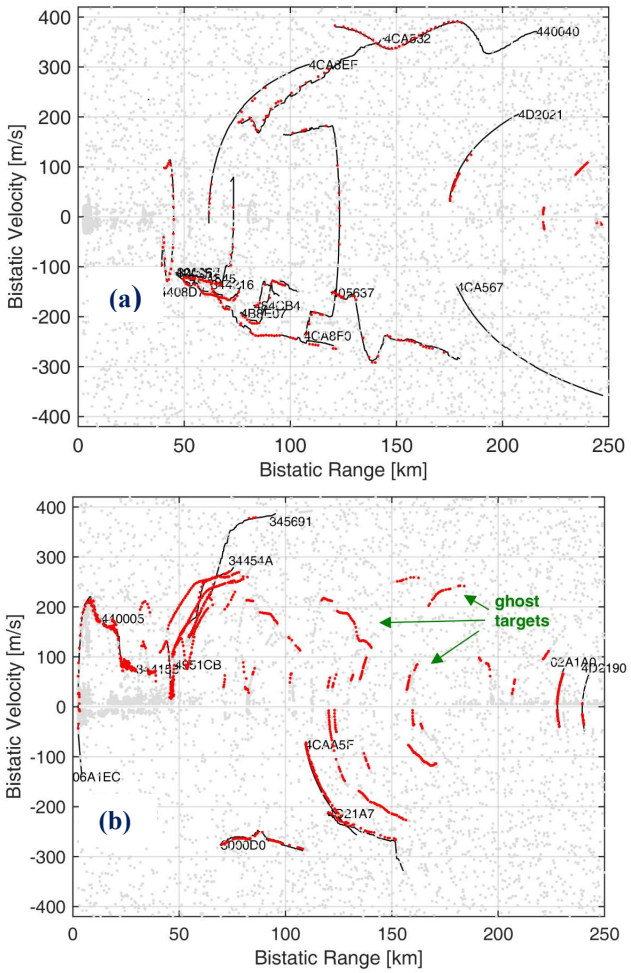

Fig. 6. *Long range detection results for: (a) Dataset 2 (b) Dataset 3.*

From Fig. 5(a) we observe that, at the time of the selected scan, both drones were flying in the monitored area with a bistatic range greater than 4 km and opposite bistatic velocities (see the red and green GPS trajectories). Two high peaks with SNR values of 25.1 dB and 23.46 dB are clearly visible around the Mavic and Phantom GPS tracks, respectively. Simultaneously, a well-focused peak with SNR=13.71 dB is present at further distance and at very high velocity (Fig. 5(b)), around the bistatic location [160 km, 359 m/s], which is likely to correspond to the aircraft return (see ADSB track in white). Incidentally, we notice that, in both figures, many other peaks appear. These can be caused by undesired contributions, such as sidelobes of the ambiguity function, disturbance residuals as well as other noise sources, or they can correspond to other targets moving in the considered area. All the peaks are equally treated but, as these maps undergo the CFAR detection stage, only the highest peaks will exceed the threshold thus yielding a raw detection.

A number of studies have demonstrated the effectiveness of a DVB-T based PR for air traffic surveillance [6]-[9]. In this work, we focus on its capability in simultaneous detecting and localizing drones and aircraft.

As an example, Fig. 6(a)-(b) report the long-range detection results over the bistatic Range-velocity plane obtained for the Datasets 2 and 3, respectively. In all cases, the DVB-T channel at F0=570 MHz is exploited and the signals from two surveillance antennas are employed after a 2-out-of-2 detection criterion across the surveillance channels. In detail, all the detection results obtained along 50 consecutive scans have been reported. In each figure, the grey dots represent all the raw detections of the passive sensor within the considered acquisition time (i.e. the detection results across all the available scans have been reported in the plot) while in black we report the available ADSB. Eventually, the red plots represent the output of the tracking stage.

By observing Fig. 6, we notice that the system is able to detect most of the aircraft flying in the surveyed area. Specifically, targets at bistatic ranges up to 150 km are detected with a remarkable continuity. Moreover, many others targets are detected with good continuity at further distances, e.g. up to 240 km. Also some ghost targets are present mainly due to the single frequency network (SFN) transmission mode (see green arrows). Several approaches could be adopted to mitigate the effect of ghost tracks formation either operating at a post-processing stage [20]-[21] or exploiting multiple DVB-T channels [8]. Finally, note that the acquisition time distance between consecutive data files (see Table 2) in Dataset 3 is smaller than in Dataset 2. This yields a higher update rate for the results in Fig. 6(b) with respect to Fig. 6(a), which in turn results in improved tracking.

The short-range results simultaneously obtained at each of the two considered tests are shown in Figs 8-9. In this case, also the results obtained for the first Dataset have been reported in Fig. 7. In each figure, sub-figure (a) illustrates the detection results in the bistatic range-Doppler domain. Correspondingly, sub-figure (b) reports the results of the targets localization in Cartesian coordinates obtained by employing, in each case, just two of the available surveillance antennas. As for Fig. 6 , grey dots have been employed to plot the raw detection results from the passive radar obtained across the considered 50 consecutive scans while we report in red and green the Mavic and Phantom GPS trajectories, respectively. Eventually, red and green plots are employed to plot the correct target detections, namely the detections associated to the Mavic and Phantom GPS, respectively.

First of all we observe that both drones are continuously detected along their trajectories from a minimum distance of 1.6 km up to a maximum distance of 5 km bistatic range across the different tests performed (see Figs 7-9(a)). This is indeed a remarkable result and successfully demonstrates the sensitivity of the employed system and the effectiveness of the adopted signal processing strategies. Furthermore, it is worth recalling that such results can be obtained while providing continuous monitoring of the aerial traffic flying at several tens of kilometres from the receiver site thus proving the sought capability of a joint short and long range surveillance.

When the drones flew at a shorter distance from the receiver, both targets were detected with a notable continuity along the acquisition time (see Fig. 7(a)). The corresponding localization results in Fig. 7(b) show that the system is also able to localize both targets with very high accuracy. However, an ambiguous plot is observed for the Mavic drone as highlighted by the green circle. In fact, for the considered DVB-T channel at carrier frequency 570 MHz, when two surveillance antennas at distance d=0.63 m are employed, the target DoA is estimated unambiguously only in an angular sector equal to 49.34° (green dotted lines in Fig. 7(b)). Notice

This paper is a postprint of a paper submitted to and accepted for publication in IET Radar Sonar and Navigation and is subject to Institution of Engineering and Technology Copyright.
The copy of record is available at the IET Digital Library.

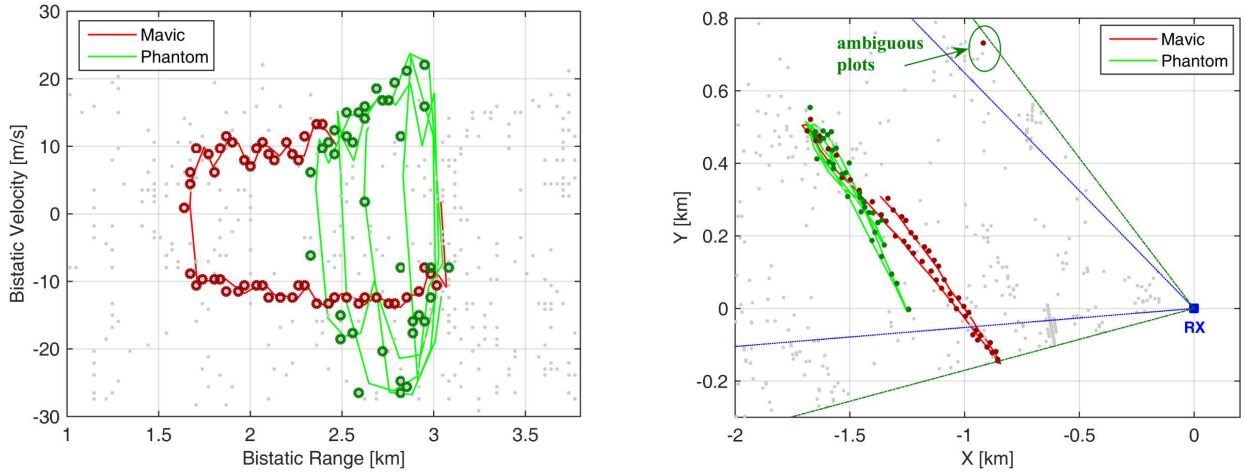

Fig. 7. *Short-range results – Dataset1: (a) Detection results; (b) Localization results.*

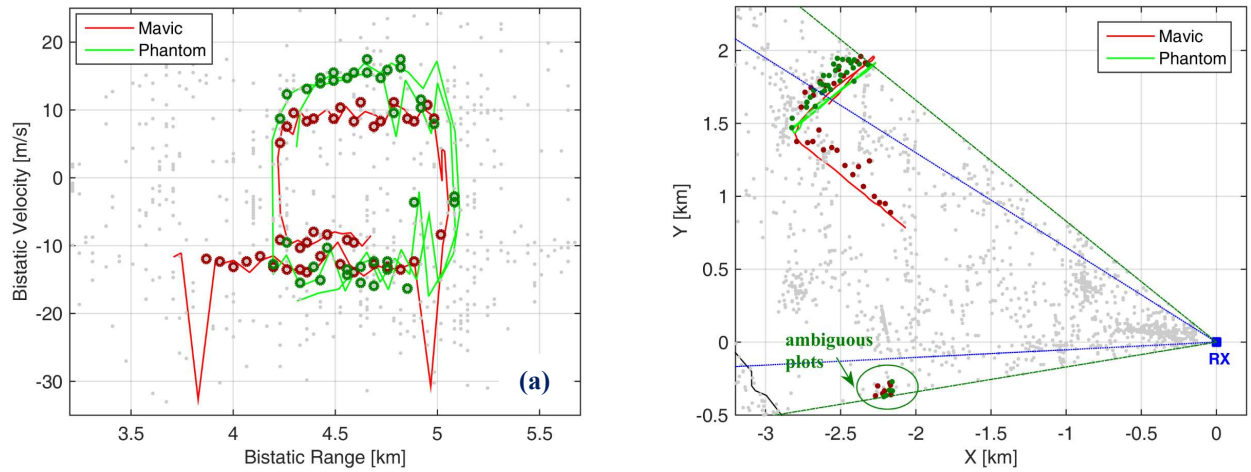

Fig. 8. *Short-range results – Dataset2: (a) Detection results; (b) Localization results.*

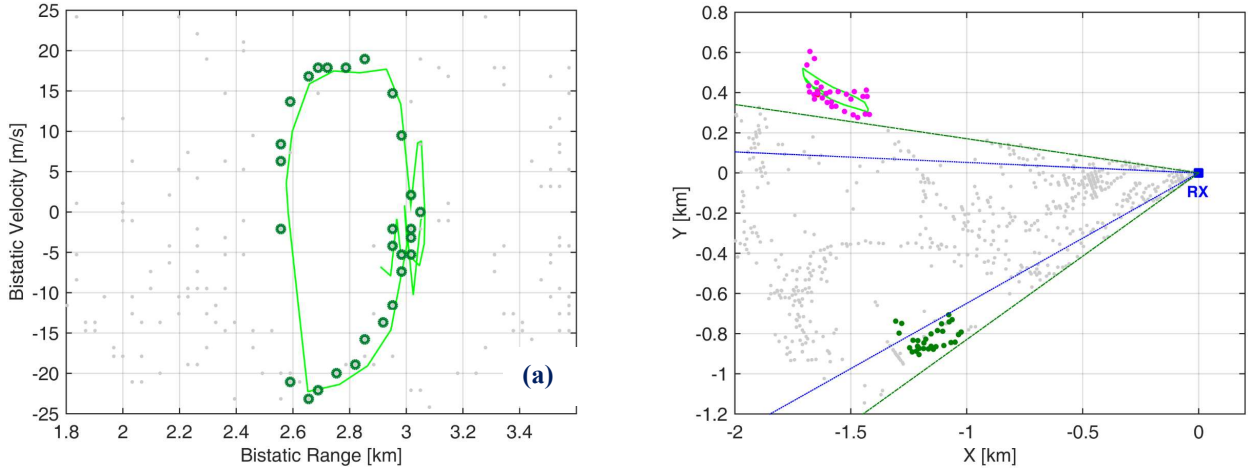

Fig. 9. *Short-range results – Dataset3: (a) Detection results; (b) Localization results.*

that the obtained unambiguous angular sector is slightly larger than the antenna main beam width of approx. 36° (blue dotted lines in Fig. 7(b)). As a consequence, the target flying just outside the unambiguous sector are likely to be detected but the corresponding plots are mis-localized in the Cartesian domain.

As the drone's distances increase (Dataset 2), we observe some missed detections (see Fig. 8(a)) and a less accurate localization capability is obtained (Fig. 8(b)). This is because the target SNR decreases thus yielding a degraded DoA estimation accuracy. This, in turn, determines higher positioning errors as the small objects move away from the receiver position. In addition, a large number of ambiguous plots are observed for the considered cases.

This effect gets worse when Dataset 3 is considered (see Fig. 9). In the reported test, the Phantom flew totally outside of the surveillance antenna main beam. On one hand, this demonstrates that the small target can still be detected with a good continuity although its

(a) **(b)**

This paper is a postprint of a paper submitted to and accepted for publication in IET Radar Sonar and Navigation and is subject to Institution of Engineering and Technology Copyright.
The copy of record is available at the IET Digital Library.

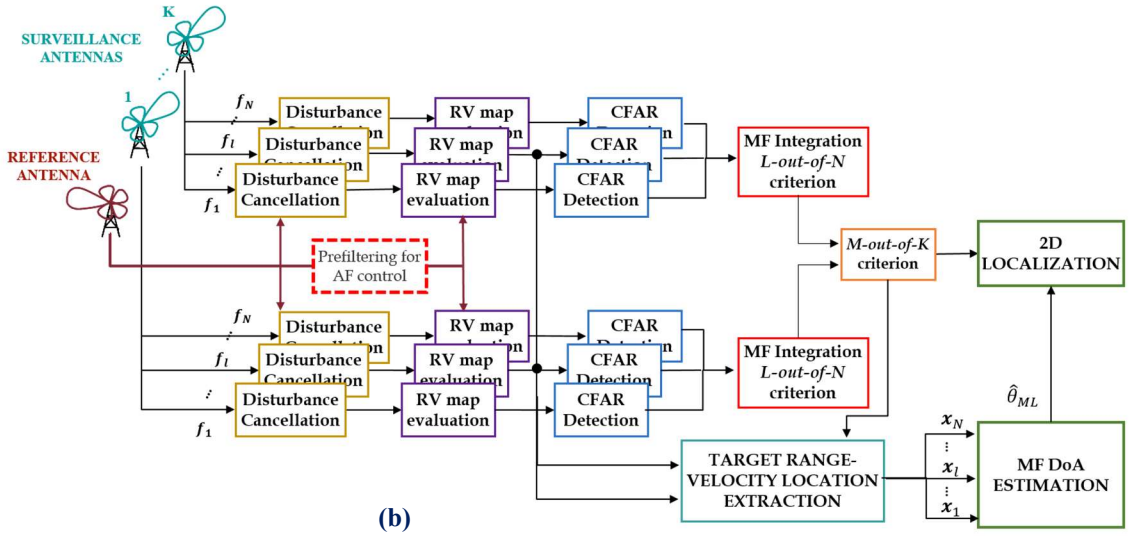

Fig. 10. *Multi-channel DVB-T based processing scheme for target detection and localization.*

reflections impinge on the sidelobes of the surveillance antennas. However, as the drone location falls outside the unambiguous angular sector, the passive plots are totally mis-localized (see the green plots in Fig. 9(b)). For illustrative purpose only, by properly compensating for the a priori known target DoA ambiguity error, the drone is correctly localized, as shown by the magenta plots in Fig. 9(b).

Apparently the effect of the angular ambiguity potentially applies to other plots provided by the PR sensor, i.e. to all the detections resulting from targets laying outside the unambiguous sector. Also, all the false alarms are projected into the Cartesian domain within the same region. This might result in a dense distribution of plots within a small angular sector which might jeopardize the subsequent tracking stage. We observe that, in order to widen the unambiguous sector, the surveillance antennas should be mounted at a shorter distance but this would yield degraded localization capability if a few antenna elements are exploited.

In the following section, we devise appropriate techniques aiming at further enhancing the performance of the system both in terms of target detection and localization. Specifically, a proper strategy is proposed to mitigate the effect of ambiguous DoA estimation while guaranteeing remarkable accuracy for targets within the antenna main-lobe.

Before concluding this section, we investigate in Table 3 the impact of the disturbance cancellation stage on the obtained performance against drone targets. Specifically, Table 3 summarizes the number of correct detections obtained with the adopted ECA-S approach and other two different cancellation strategies (namely, no cancellation and conventional ECA) for the same case studies of Fig. 7-9(a). The results clearly show that the disturbance cancellation stage is an essential block for the detection of such targets. We observe that the use of ECA and ECA-S allows a significant enhancement in target detection compared to the case of no disturbance cancellation. Moreover, the ECA-S yields a further improvement over the conventional ECA since it has been shown to be more robust to the time-varying characteristics of the environment [17],[22]. As expected, the advantage of ECA-S becomes more evident when lower SNR targets are considered. This is the case of Dataset3 (the Phantom flew totally outside of the surveillance antenna main beam) where the ECA-S yields an enhancement of the number of correct detections of about 20% with respect to the conventional ECA.

5. Multi-channel strategies to improve the detection and localization performance

As it is well known, target detection (b) mance depends highly on the selected transmitter of opportunity and, in particular, it significantly varies with the employed DVB-T channel. In fact, both the radiating characteristics of the transmitter and the electromagnetic conditions of the propagation channel vary across the wide frequency band allocated to the DVB-T service in the UHF band (from 470 MHz to 862 MHz). In addition, also the target scattering can change with the different considered frequency channels. Eventually, target DoA estimation is characterized by low accuracies even operating at UHF band. Moreover, as mentioned in the previous section, when we operate with a uniform linear array (ULA), the requirements of accurate DoA estimation and wide unambiguous angular sector sets competing constraints on the array equivalent length.

In this work, to overcome the aforementioned limitations, we take advantage of the frequency and spatial diversity allowed by the multi-frequency operation and a non-uniform linear array layout.

Table 3. Comparison of the detection results obtained for the case studies of Figs 7-9(a) with different cancellation strategies.

	No disturbance cancellation		**ECA**		**ECA-S**	
	Mavic	Phantom	Mavic	Phantom	Mavic	Phantom
Dataset 1	25	3	48	34	50	35
Dataset 2	0	0	39	33	39	35
Dataset 3	-	0	-	26	-	33

This paper is a postprint of a paper submitted to and accepted for publication in IET Radar Sonar and Navigation and is subject to Institution of Engineering and Technology Copyright.
The copy of record is available at the IET Digital Library.

Table 4. Datasets 1 & 2: comparison of the SF and the MF configurations (over 50 scan) using two and three surveillance antennas.

		Mavic				Phantom			
		Nº of detection		Ambiguous plots		Nº of detection		Ambiguous plots	
		2 surv	3 surv	2 surv	3 surv	2 surv	3 surv	2 surv	3 surv
Dataset 1	**SF F0**	50	50	1	0	35	37	0	0
	SF F1	50	50	9	0	38	36	0	0
	MF DEC 1/2	50	50	0	0	38	37	0	0
Dataset 2	**SF F0**	39	42	7	0	35	36	5	0
	SF F1	30	32	11	0	42	41	24	0
	MF DEC 1/2	41	43	2	0	41	40	0	0

Specifically, aiming at improving the target detection capability and the reliability of the considered system, we consider the joint exploitation of multiple DVB-T channels emitted by the same broadcast illuminator of opportunity based on the detection schemes proposed in [8]. Among the different MF operation approaches, the decentralized detection scheme (MF DEC) is adopted in the following since it has been shown to be more robust to the presence of ghost targets or unwanted plots formations. Therefore, a detection is declared at a given range/velocity location when L detections out of N available frequency channels are obtained for the considered range-Doppler bin $[l_0, m_0]$ of the maps separately evaluated at each surveillance channel. Specifically, by defining $\mathrm{b}_n[l_0, m_0]$ the binary map at the output of the CFAR detection stage of Fig. 4, we obtain:

$$\sum_{n=1}^{N} \mathrm{b}_n[l_0, m_0] \underset{H_0}{\overset{H_1}{\gtrless}} L \tag{2}$$

In this case, a conventional CA-CFAR threshold is separately applied at each single frequency channel in order to achieve the desired P_{fa} after the MF binary integration:

$$P_{fa} = \sum_{i=L}^{N} \binom{N}{i} P_{fa}^{SF\,i} \left(1 - P_{fa}^{SF}\right)^{N-i} \tag{3}$$

where P_{fa}^{SF} is the probability of false alarm set at each DVB-T channel. Once the target has been detected on the range-velocity plane, the DoA of the corresponding echo has to be estimated with the purpose of localizing it in the X-Y plane. To this purpose, we take advantage MF operation in conjunction with a non-uniform linear array (NULA) layout in order to relax the trade-off between DoA estimation accuracy and unambiguous angular sector. In detail, we resort to a ML approach that incoherently integrates the target echoes at multiple carrier frequencies. Specifically, the ML estimate of the target DoA $\hat{u}_{ML} = \sin(\hat{\vartheta}_{ML})$ (ϑ being the angle of arrival, measured relative to the array boresight) is obtained as:

$$\hat{u}_{ML} = \underset{u}{\operatorname{argmax}} \sum_{n=1}^{N} \frac{1}{\sigma_n^2} |\boldsymbol{s}_n^H(u)\boldsymbol{x_n}|^2 \tag{4}$$

where $\boldsymbol{x}_n$ is the N x1 vector with the complex values extracted at the range-velocity location where the target has been detected, σ_n^2 is the noise power at the n-th frequency channel while $\mathbf{s}_n(u)$ is the spatial target steering vector. For a linear array composed by K surveillance antennas at positions d_k $(k = 0,..,K-1)$ measured with respect to the phase reference point, $\mathbf{s}_n(u)$ is given by:

$$\mathbf{s}_n(u) = \left[e^{j\frac{2\pi}{\lambda_n}d_0 u} \quad \ldots \quad e^{j\frac{2\pi}{\lambda_n}d_{K-1}u}\right]^H \tag{5}$$

where λ_n is the n-th wavelength, n=1,..,N.

This approach benefits from the increased equivalent target SNR provided by the MF integration, which yields enhanced estimation accuracy for unambiguous targets. However, along with this expected advantage, the frequency diversity and the non-uniform spacing of the receiving antenna elements allow to build up an improved ML likelihood function with reduced sidelobes level. Therefore, the probability of outliers in target DoA estimation is lowered even operating with few and largely spaced antenna elements [23].

The processing scheme to be applied at each branch of the architecture in Fig. 4 is sketched in Fig. 10.

6. Performance improvement with the multi-channel strategies

The effectiveness of the approaches summarized in the previous section has been largely demonstrated against conventional air traffic for medium and long range surveillance applications [8], [14].

In this section we illustrate the benefits gained for the considered counter drone operations both in terms of target detection capability and localization accuracy. Specifically, we focus on Datasets 1 and 2 due to the availability of both multiple DVB-T frequency channels and surveillance antennas. The same case studies of Figs 7 and 8 are considered.

First we consider the use of two surveillance antennas. Table 4 reports a quantitative comparison in terms of number of correct detections and number of mislocalized plots (due to DoA estimation ambiguities) when separately exploiting the two frequency channels and after the MF operation. In detail, we employ the MF decentralized detection scheme based on a 1-out-of-2 strategy (MF DEC 1/2) while the ML approach in eq. (4) is considered for DoA estimation. Specifically, the maximization of (4) is performed over a wide angular sector equal to [-50°:0.01°:50°]. It is worth noticing that this sector is wider than the unambiguous sector

This paper is a postprint of a paper submitted to and accepted for publication in IET Radar Sonar and Navigation and is subject to Institution of Engineering and Technology Copyright.
The copy of record is available at the IET Digital Library.
that is guaranteed given the distance among the employed antennas on receive, with both the considered carrier frequencies.

By observing Table 4 we notice that the two DVB-T channels yield comparable detection results when the drones flew at a shorter distance (Dataset 1). In detail, it is interesting to note that the Mavic drone is detected with a detection rate equal to 100% over the available 50 scans. In this case, for both drones, due to the comparable and remarkable detection performance of both single channels, we observe that the MF operation does not yield any significant improvement in terms of target detection capability with respect to the single frequency operation. In contrast, the possibility to widen the unambiguous angular sector provided by the MF approach, allows to correctly localize all plots in the Cartesian plane (see Table 4 and Fig. 11(a)) even operating with two surveillance antennas.

When the distance of the drones increases (Dataset 2), we observe that the target detection capability shows a larger dependency with the employed DVB-T channel. Moreover, the best performing DVB-T channel varies with the two drones. In this case, the detection performance improvement provided by the MF approach is quite apparent as many additional plots are obtained with respect to the worst single frequency operation of each target. In addition, the MF solution avoids the ambiguous estimation of the DoA for targets flying outside the unambiguous angular sector provided by the SF operation. However, there is a non-zero probability that outliers could occur when two antennas are considered. In fact, in the considered test, two ambiguous plots are obtained as highlighted by the green circle in Fig. 12(a).

This paper is a postprint of a paper submitted to and accepted for publication in IET Radar Sonar and Navigation and is subject to Institution of Engineering and Technology Copyright.
The copy of record is available at the IET Digital Library.

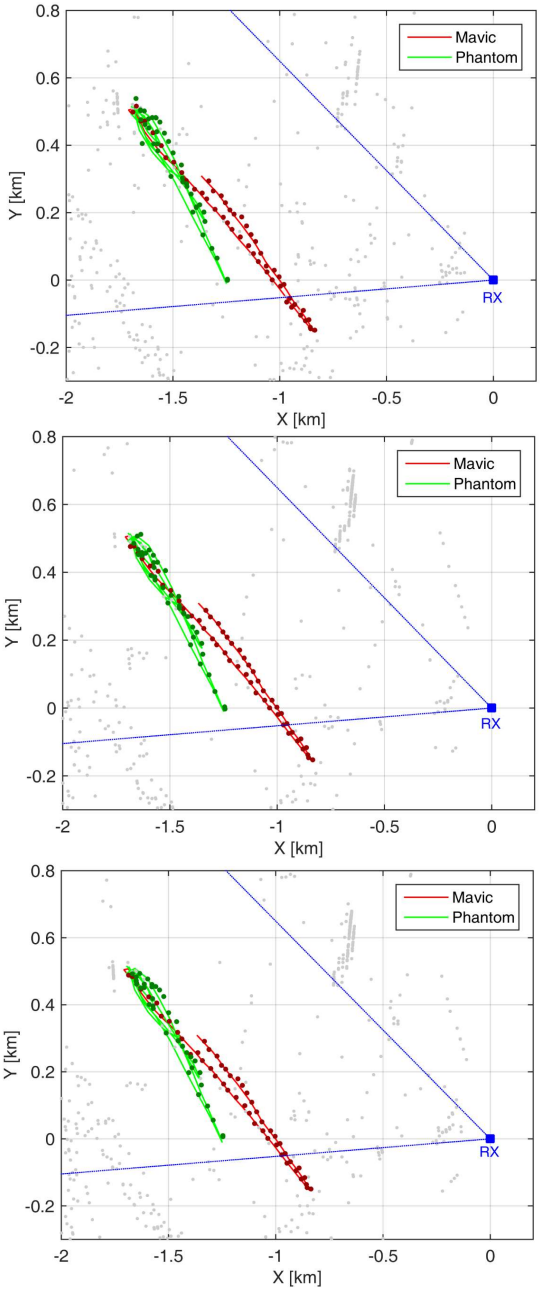

Fig. 11. *Dataset 1: Localization results for 50 consecutive data files using*

(a) MF DEC 1/2 with 2 surveillance antennas;
(b) SF F0 with 3 surveillance antennas;
(c) MF DEC 1/2 with 3 surveillance antennas.

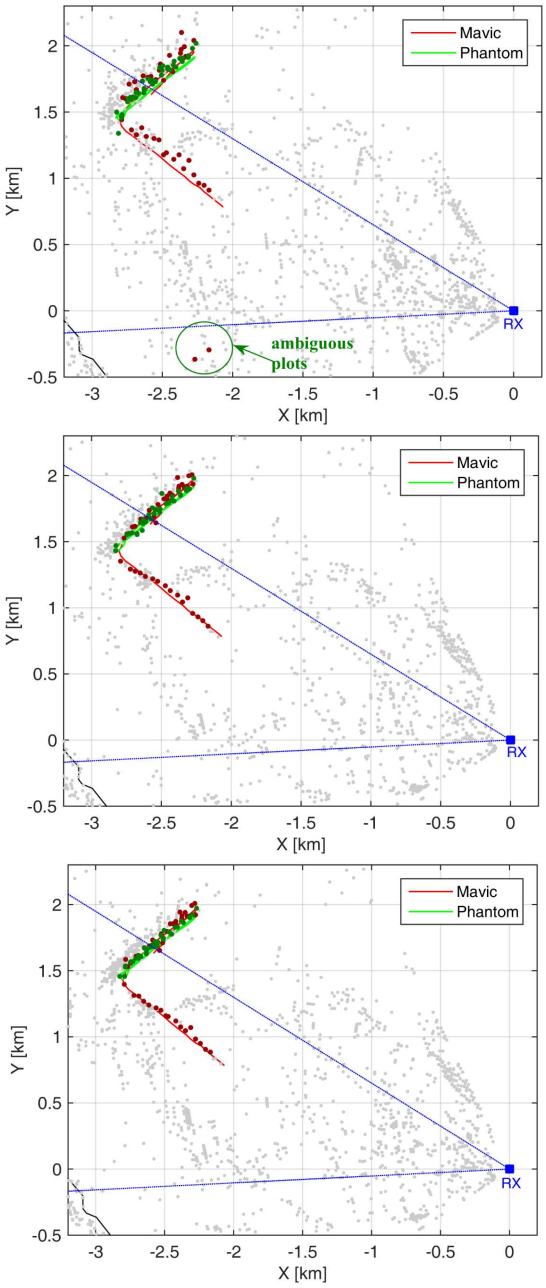

Fig. 12. *Dataset 2: Localization results for 50 consecutive data files using*

(a) MF DEC c 1/2 with 2 surveillance antennas;
(b) SF F0 with 3 surveillance antennas;
(c) MF DEC 1/2 with 3 surveillance antennas.

Alternatively, in order to increase at the same time both the DoA estimation accuracy and the unambiguous angular sector, a NULA can be used. The number of correct detections and mis-localized plots for both DVB-T channels, for the case of three surveillance antennas, are illustrated in Table 4. As an example, Figs 11-12(b) report the localization results when using three surveillance antennas and the single frequency F0. By comparing the results obtained with two and three surveillance antennas, it is evident that in all cases the exploitation of three antennas allows to correctly localize all plots in the Cartesian plane (namely, zero ambiguous plots). Moreover, by comparing Figs 11-12(b) with Figs 7-8(b), we might notice that the use of three antennas allows more accurate localization. This is apparent especially at longer distance from the RX where a reduced DoA estimation accuracy is expected with the SF operation which in turn results in a degraded localization capability due to the projection of the angular errors in the Cartesian domain.

Eventually, a further improvement in terms of localization results might be achieved by jointly exploiting multiple frequency channels and surveillance antennas (Figs 11-12(c)). In this case, when three surveillance antennas are used, the MF operation allows only a slight improvement in the localization accuracy with respect to the SF approaches. Notice that the localization improvement does not appear substantial against the considered targets since remarkable

This paper is a postprint of a paper submitted to and accepted for publication in IET Radar Sonar and Navigation and is subject to Institution of Engineering and Technology Copyright.
The copy of record is available at the IET Digital Library.

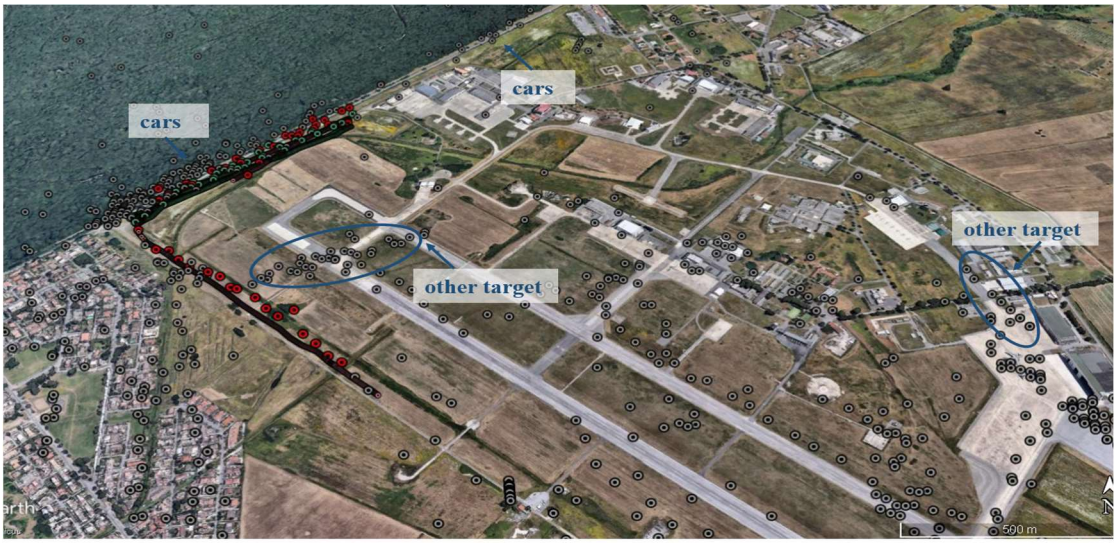

Fig. 13. *Dataset2: localization results of Fig. 12(c) over the Google Earth map of the local area.*

localization performance was obtained with the two single DVB-T channels.

Nevertheless, it is worth noticing that the obtained benefits also apply to other targets detected by the PR. As an example, Fig. 13 shows the localization results of Fig. 12 (c) over the Google Earth map of the local area. As it is evident, in addition to the cooperative drones, the considered system is able to detect many other targets that are likely to correspond to vehicles or aircraft moving on the surface of the airport as well as to birds (comparable with the drones in terms of size). The possibility to widen the unambiguous angular sector greatly simplifies the discrimination among tracks in the Cartesian domain. However, the reported results clearly show that the considered system is able to continuously detect several targets that could be typically encountered in an airport scenario. Therefore, in order to make the DVB-T based PR sensor able to distinguish among the different type of targets, proper strategies should be considered in the future.

7. Conclusion

In this paper, we investigated the effectiveness of a DVB-T based PR sensor for simultaneous counter drone operations and civil air traffic surveillance. In detail, aiming at monitoring airport terminal areas, we demonstrated that such sensor could be employed for simultaneous short and long range surveillance of drones and aircraft. For the purpose, different experimental tests have been performed with the DVB-T based AULOS® PR designed by Leonardo S.p.A. against two very small drones and conventional civil air traffic. Moreover, an appropriate processing scheme has been developed to be efficient for the twofold search task. The reported results have shown the capability of the sensor for simultaneously detecting and localizing drones flying around the airport area as well as the civil air traffic up to a few hundreds of kilometers.

Eventually, the exploitation of frequency and spatial diversity was demonstrated to provide further performance improvement by enhancing the target detection capability and widening the area where the obtained plots are unambiguously localized. These benefits have been shown to be strategic features especially in the considered short range surveillance application where multiple targets simultaneously occupy the scene. Future activities will address the exploitation of proper strategies aimed at equipping the sensor with the capability to distinguish between different classes of targets.

8. Acknowledgments

The authors would like to thank Maggiore Alfonso Masciavè of the Italian Air Force for the support in the experimental tests.

The authors also would like to thank to Dr. Alfonso Farina for his encouragement and precious suggestions.

9. References

[1] M. Ritchie, F. Fioranelli, and H. Borrion, ``Micro UAV crime prevention: Can we help Princess Leia?" in Preventing Crime in the 21st Century, B. L. Savona and Ed. Cham, Swizerland: Springer, 2017, pp. 359-376.

[2] https://www.postandcourier.com/news/report helicopter-crash-on-daniel-island-may-have-been caused/article_1123767a-12a7-11e8-bf2e 2798e681cd6b.html.

[3] https://www.newscientist.com/article/2190096-drones-are-causingairport-chaos-why-cant-we-stop-them/.

[4] X. Shi, C. Yang, W. Xie, C. Liang, Z. Shi and J. Chen, "Anti-Drone System with Multiple Surveillance Technologies: Architecture, Implementation, and Challenges," in *IEEE Communications Magazine*, vol. 56, no. 4, pp. 68-74, April 2018.

[5] K. E. Olsen and H. Kuschel, "From the editors of the special issue: Passive and multi-static radar for civil applications," in IEEE Aerospace and Electronic Systems Magazine, vol. 32, no. 2, pp. 3-3, Feb. 2017.

[6] H. Kuschel, J. Heckenbach, D. O'Hagan and M. Ummenhofer, "A hybrid multi-frequency Passive Radar concept for medium range air surveillance," *2011 MICROWAVES, RADAR AND REMOTE SENSING SYMPOSIUM*, Kiev, 2011, pp. 275-279.

This paper is a postprint of a paper submitted to and accepted for publication in IET Radar Sonar and Navigation and is subject to Institution of Engineering and Technology Copyright.
The copy of record is available at the IET Digital Library.

[7] D. Poullin and M. Flecheux, "Passive 3D tracking of low altitude targets using DVB (SFN Broadcasters)," in IEEE Aerospace and Electronic Systems Magazine, vol. 27, no. 11, pp. 36-41, November 2012.

[8] T. Martelli, F. Colone, E. Tilli, and A. Di Lallo, "Multi-Frequency Target Detection Techniques for DVB-T Based Passive Radar Sensors," in Sensors 2016, Sept. 2016.

[9] F. Pignol, F. Colone and T. Martelli, "Lagrange-Polynomial-Interpolation-Based Keystone Transform for a Passive Radar," in *IEEE Trans. on AES*, vol. 54, no. 3, pp. 1151-1167, June 2018.

[10] Y. Liu, X. Wan, H. Tang, J. Yi, Y. Cheng and X. Zhang, "Digital television based passive bistatic radar system for drone detection," IEEE Radar Conference 2017, Seattle, WA, 2017, pp. 1493-1497.

[11] D. Poullin, "Countering illegal UAV flights: passive DVB radar potentiality," International Radar Symposium 2018, Bonn, pp. 1-10.

[12] M. P. Jarabo-Amores et al., "Drone detection feasibility with passive radars," European Radar Conference 2018, Madrid, Spain, pp. 313-316.

[13] T. Martelli, F. Colone, and R. Cardinali, "Simultaneous short and long range surveillance of drones and aircrafts with DVB-T based Passive Radar," to be presented at 2019 International Radar Conference, 23-27 Sept. 2019, Toulon (France).

[14] F. Filippini, T. Martelli, F. Colone and R. Cardinali, "Target DoA estimation in passive radar using non-uniform linear arrays and multiple frequency channels," *IEEE Radar Conference 2018*, Oklahoma City, OK, pp. 1290-1295.

[15] F. Filippini, T. Martelli, F. Colone, T. Martelli, R. Cardinali, "Exploiting long coherent integration times in DVB-T based passive radar systems," IEEE Radar Conference 2019, Boston (USA).

[16] M. I. Skolnik, Ed., *Introduction to Radar Systems*, 3rd ed. New York, NY, USA: McGraw-Hill, 2001.

[17] F. Colone, C. Palmarini, T. Martelli, E. Tilli, "Sliding extensive cancellation algorithm for disturbance removal in passive radar," in IEEE Trans. on AES, vol. 52, no. 3, pp. 1309-1326, June 2016.

[18] F. Colone, D. Langellotti, P. Lombardo, "DVB-T signal ambiguity function control for passive radars," in IEEE Trans. on AES, vol. 50, no. 1, pp. 329-347, Jan. 2014.

[19] P. Lombardo, F. Colone, "Advanced processing methods for passive bistatic radar systems", chapter in the book edited by W. L. Melvin and J. A. Scheer, "Principles of Modern Radar: Advanced Radar Techniques", SciTech Publishing, Inc., 2012.

[20] M. Daun and W. Koch, "Multistatic target tracking for non-cooperative illumination by DAB/DVB-T," 2008 IEEE Radar Conference, Rome, 2008, pp. 1-6

[21]] M. Daun, "Deghosting in passive air surveillance systems," 11-th INTERNATIONAL RADAR SYMPOSIUM, Vilnius, 2010, pp. 1-8.

[22] T. Martelli, R. Cardinali and F. Colone, "Detection performance assessment of the FM-based AULOS® Passive Radar for air surveillance applications," 2018 19th International Radar Symposium (IRS), Bonn, 2018, pp. 1-10.

[23] F. Filippini, F. Colone and A. De Maio, "Threshold Region Performance of Multi-Carrier Maximum Likelihood Direction of Arrival Estimator," in *IEEE Trans. on AES.*